Upper limits to surface-force disturbances on LISA proof masses and the possibility of observing galactic binaries

Ludovico Carbone, Giacomo Ciani, Rita Dolesi, Mauro Hueller, David Tombolato, Stefano Vitale, and William Joseph Weber

Department of Physics, University of Trento and INFN, Gruppo Collegato di Trento, I-38050, Povo, Trento, Italy

Antonella Cavalleri

Istituto di Fotonica e Nanotecnologie CNR-ITC and INFN, Gruppo Collegato di Trento, I-38050 Povo, Trento, Italy

(Received 5 November 2006; published 12 February 2007)

We have measured surface-force noise on a hollow replica of a LISA proof mass surrounded by its capacitive motion sensor. Forces are detected through the torque exerted on the proof mass by means of a torsion pendulum in the 0.1–30 mHz range. The sensor and electronics have the same design as for the flight hardware, including 4 mm gaps around the proof mass. The measured upper limit for forces would allow detection of a number of galactic binaries signals with signal-to-noise ratio up to ≈ 40 for 1 yr integration. We also discuss how LISA Pathfinder will substantially improve this limit, approaching the LISA performance.

DOI: 10.1103/PhysRevD.75.042001 PACS numbers: 04.80.Nn, 07.87.+v, 95.55.Ym

I. INTRODUCTION

LISA is a space-borne interferometric gravitational wave detector under development by the American (NASA) and European (ESA) space agencies [1]. The detector measures the gravitational wave-induced change in the distance between free-falling proof masses (PM) separated by $\approx 5 \times 10^9$ m. Three PM pairs define three lines that form a nearly equilateral triangle.

The PM pairs are in pure geodesic motion, free of spurious *relative* acceleration noise along the measurement axis (referred to as x from now on) to within $\sqrt{2} \times \{3 \times 10^{-15}\ (\mathrm{m/s^2}\sqrt{\mathrm{Hz}})\sqrt{1 + (f/3\ \mathrm{m\,Hz})^4}\}$, where f is the frequency.

The PMs in LISA are cubes made of a Au-coated Au-Pt alloy with no mechanical contact to the surroundings. Disturbing forces act mainly on the surface, while the bulk is affected by low frequency magnetic and gravitational effects.

The magnetic fields due to spacecraft and the PM magnetic properties can both be measured on the ground with sufficient accuracy, and thus the magnetic force noise expected in flight can be well characterized. The interplanetary magnetic field is known to be stable enough to be a minor entry in the LISA error budget [2].

Gravitational noise is expected to be due to spacecraft thermo-mechanical distortion. This is being modeled as part of the development of LISA Pathfinder (LPF) mission, the LISA precursor under development by ESA [3], and the predicted gravitational noise will be tested in flight.

Surface forces include, for instance, low frequency electric field fluctuations, thermal radiation effects, and residual pressure gradients. These forces are the most difficult to model, as they may be connected, for instance, to electrochemical or radiative properties of surfaces.

In LISA the PM is surrounded by a set of electrodes used to detect the PM motion within the spacecraft. Six pairs of electrodes are used to sense motion in all degrees of freedom (DOF), using 100 kHz capacitance bridge readouts. In addition a set of biasing electrodes on opposing faces along one or both directions normal to x provides the PM ac-voltage polarization required by the bridge to work. The position information is fed back to control loops that suppress relative spacecraft-PM motion.

We call this electrode system, its support housing, the readout coaxial cables, and other accessories, the gravity reference sensor (GRS). The GRS creates a nearly closed cavity around the PM, and, with its Au-coated electrodes and housing, serves as an electrostatic shield. Thus the GRS shields the PM from external sources of surface force and is, in practice, the dominant source of surface-force disturbances.

We proposed [4] a torsion pendulum to investigate surface forces on LISA-like PMs and we ran [5] a first experimental campaign on a prototype GRS with a 40 mm size cubic test-mass surrounded by 2 mm gaps to the surrounding sensor electrode surface. That campaign put a first upper limit on nonmodeled surface forces acting within the GRS. This upper limit was obtained by comparing the pendulum noise to its estimated intrinsic thermal noise background.

At the time no independent estimate of the angular measurement noise was performed, and as such this noise source was not included in the background estimate used for establishing a force noise upper limit.

In the subsequent development of the LPF mission [3], the design of the GRS has evolved into the final version to be implemented for the flight [6]. The test-mass is now 46 mm, and gaps around it have been widened in order to further suppress surface disturbances. We have manufactured a prototype of this flight design and have run a new experimental campaign on it.

In addition we have found a new technique that allows now for discriminating in the data the contribution of the real torque on the test-mass from readout and other additive noise. In this paper we present the results of this new testing campaign and compare them with the requirements for the LISA mission.

Finally we also compare these results with the expected performance of a very much related experiment, the full in-flight test of LISA PM on LPF. In doing so we present the expected leading sources of noise in that mission and the further projected improvement it will achieve in putting an upper limit on nonmodeled stray forces.

II. EXPERIMENTAL

A. GRS design and torsion pendulum main features

The first measurement campaign [5] employed a prototype sensor with a hollow, 40 mm Au-coated titanium PM, suspended in axis with a W wire, and, as mentioned, with 2 mm gaps to the surrounding sensor electrode surfaces. The hollow PM allows use of a thinner torsion fiber, and thus higher force sensitivity, than with the full 2 kg LISA PM, without sacrificing representativity for surface forces [4,5]. The electrodes were Au-coated Mo plates, with biasing electrodes only along one axis (the z-axis). A homemade readout electronics was used for the measurements.

The design for the GRS to be flown on the LPF mission [3] has changed [6]. The electrodes are now Au-coated ceramic pieces mounted inside a Mo structure. In addition the biasing electrodes are present on all faces except the ones along x.

The PM is now a 46 mm cube, separated from the electrodes by a gap of 4 mm along the x-direction, and 2.9 mm and 3.5 mm on the other axes. Wider gaps have been adopted because forces connected with stray dc-potentials on metal surfaces, also known as ''charge patches'' decay with the gap width d with a functional form that depends on the specific noise mechanism such as coupling to the PM charge, the direct coupling between patch fields, dielectric losses, and force gradients. Some of these effects may decay as d^{-3} or even more rapidly [7]. Thus widening gaps by a factor 2 may entail a potential suppression of this disturbance by almost an order of magnitude for certain effects.

In addition the ratio between the cross sectional area for gas flow around the PM in the x-direction and the area of the x-face electrodes has increased by 50%. This ratio enters in suppressing the effect of a possible pressure gradient due to asymmetric outgassing around the PM [6].

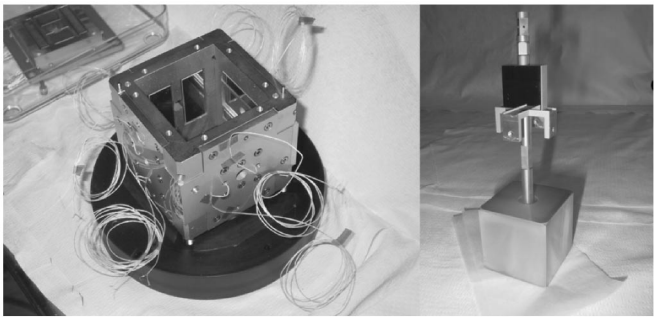

FIG. 1. Left: the electrode housing of the GRS. The electrodes for the x-direction motion readout are the pair of shiny vertical plates visible inside the sensor. On the adjacent y-face, there is a y-sensing electrode, the upper horizontal plate, and one of the electrodes used to polarize the proof mass for capacitive readout. Right: the hollow proof mass used for the torque measurements.

We have performed a new measurement campaign on a prototype of this new sensor design, connected to readout electronics closely following the final flight-hardware design.

The main features of the prototype are described above, with a photograph shown in Fig. 1. Details of the readout scheme can be found both in Refs. [5,6]. Also shown in Fig. 1 is the pendulum inertial element, featuring a 46 mm hollow Al cube suspended by a W wire by means of an Al shaft. The shaft is electrically isolated from the PM via a quartz ring hidden underneath the top face of the PM. A mirror used for the independent optical readout of the angular motion is attached to the shaft, along with a structure used to balance the entire setup. The total moment of inertia $I_o = (4.31 \pm 0.01) \times 10^{-5}$ kg m^2. The PM is suspended under high vacuum (10^{-5} Pa).

The resulting torsional oscillator has a period approximately $T_o = 564$ s and a quality factor $Q = 2900 \pm 500$.

The GRS is mounted on a μm precision manipulator that allows moving and centering it around the PM, to which it has no mechanical contact.

The pendulum motion is measured both by the GRS and by an optical readout based on a commercial autocollimator (Möller-Wedel ELCOMAT vario 300/D40). The GRS has a sensitivity of order 2 nm/$\sqrt{\text{Hz}}$ in displacement and 200 nrad/$\sqrt{\text{Hz}}$ in rotation above 1 mHz for all DOF. The autocollimator has an intrinsic resolution of 20 nrad/$\sqrt{\text{Hz}}$ above 1 mHz.

B. EVALUATION OF TORQUE AND BACKGROUND SUBTRACTION

The angular motion of the pendulum $\phi(t)$ is converted into an instantaneous applied torque $N(t)$ as

$$N(t) = I_o\{\ddot{\phi}(t) + (2\pi/T_oQ)\dot{\phi}(t) + (2\pi/T_o)^2\phi(t)\}. \quad (1)$$

The derivatives are estimated from a sliding second order fit to 5 adjoining data. Equation (1) approximates the damping as viscous, while in reality it is dominated by structural dissipation within the fiber. However, the difference between these two models has no detectable effect on data processing.

In order to get an estimate of the expected readout background noise, we formed the average, $\bar{N}(t) = [N_{\rm GRS}(t) + N_{\rm ac}(t)]/2$, and semidifference, $\delta N(t) = [N_{\rm GRS}(t) - N_{\rm ac}(t)]/2$, of the torques, $N_{\rm GRS}(t)$ and $N_{\rm ac}(t)$, calculated, respectively, from the GRS and autocollimator angular readouts $\phi_{\rm GRS}(t)$ and $\phi_{\rm ac}(t)$. For ideally uncorrelated readout noise, the power spectral densities (PSD) of these signals should be:

$$S_{\bar{N}}(f) = S_N(f) + \frac{S_{n,\phi_{\rm GRS}}(f) + S_{n,\phi_{\rm ac}}(f)}{4|H(f)|^2};$$
$$S_{\delta N}(f) = \frac{S_{n,\phi_{\rm GRS}}(f) + S_{n,\phi_{\rm ac}}(f)}{4|H(f)|^2}, \qquad (2)$$

where $S_x(f)$ is the PSD of process x at frequency f, $S_{n,\phi_{\rm GRS}}(f)$ and $S_{n,\phi_{\rm ac}}(f)$ are the PSDs of the uncorrelated angular readout noise of, respectively, the GRS and autocollimator, and $H(f) = \{I_o(2\pi)^2[(1/T_o)^2 - f^2 + i(f/T_oQ)]\}^{-1}$ is the pendulum torque-to-angle transfer function. Thus within this model one can estimate the torque PSD by:

$$S_N(f) = S_{\bar{N}}(f) - S_{\delta N}(f) = {\rm Re}\{S_{N_{\rm ac},N_{\rm GRS}}(f)\}. \qquad (3)$$

Equation (3) indicates that, in this model, the difference $S_{\bar{N}}(f) - S_{\delta N}(f)$, attributed to true torque noise, is equivalent to the correlated noise between the two signals, and can be calculated as the cross-spectral density (CSD) ${\rm Re}\{S_{N_{\rm ac},N_{\rm GRS}}(f)\}$ between $N_{\rm GRS}(t)$ and $N_{\rm ac}(t)$.

III. RESULTS

In Fig. 2 we report an example of the outcome of this data reduction procedure.

In this specific run an extra coupling to motion of the PM in the y-direction was detected through the correlation of $\bar{N}(t)$ with this motion as measured by the GRS. The motion is a few orders of magnitudes larger than any S/C motion relevant for LISA, and thus a small coupling converts into a large torque that would not translate into a corresponding force on a LISA PM.

We subtracted the y-signal of the GRS multiplied just by a constant from the $\bar{N}(t)$ data series managing to decrease the noise PSD by a factor 2 between 0.2 mHz and ≈ 2 mHz, with negligible effect at higher frequencies.

The constant minimizing the residual noise was found to be $\partial N/\partial y = -9.8 \pm 2.2$ nN. This number, confirmed in other runs, agrees with the results of coarse measurement obtained by moving the GRS with the micromanipulator that gives $\partial N/\partial y \approx 7$ nN. Coincident with the appearance of this extra coupling, an additional angular stiffness of

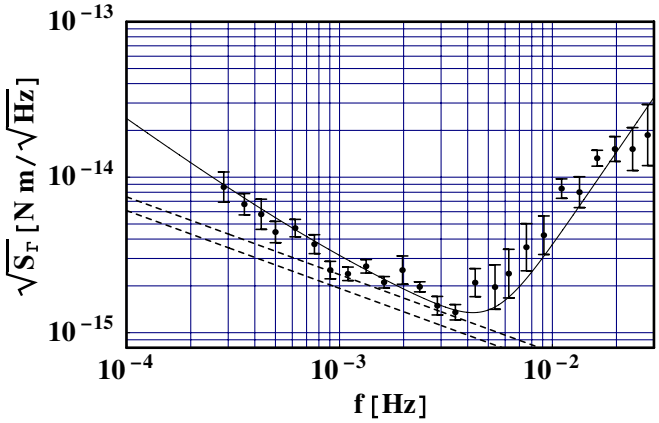

FIG. 2 (color online). Total torque noise. Data points: square root of torque noise PSD estimated from autocollimator and capacitive sensor cross correlation after time domain subtraction of the effect of PM motion along y. Values and error bars are estimated as the mean and its standard deviation of PSD data falling within the corresponding frequency bins. Bins have equal logarithmic width. Dashed lines delimit the error band for the estimate of thermal noise. The continuous smooth line is a linear least square fit to data as described in the text.

$\partial^2 N/\partial\phi^2 = (1.43 \pm 0.02) \times 10^{-10}$ Nm/rad was measured by rotating the GRS [8].

$\partial N/\partial y$ and $\partial^2 N/\partial\phi^2$ taken together, suggest a localized charged feature on the y-face at ≈ 1.5 cm from the center, compatible with the observed slow decay of the effect with time and with the presence of many observed defects in the electrode Au coating that expose the potentially charged dielectric underneath.

Figure 2 also shows the expected thermal torque noise associated with pendulum damping that provides the ultimate torque noise floor. As damping at these low frequencies is dominated by dissipation within the fiber, the expected PSD is

$$S_{\rm th}(f) = 4k_BTI_o(2\pi/T_o)^2/(2\pi fQ), \qquad (4)$$

with T the temperature and k_B the Boltzmann constant.

The residual noise coincides with the expected thermal background, within the errors, only near 1–2 mHz. In order to quantify the extra noise at other frequencies we performed a fit to the excess with a simple polynomial law of frequency in the range 0.2–30 mHz. Many different power laws were tested with linear combinations of both positive and negative exponents. The only choice giving fully significant F-test value for all terms in the polynomial is the superposition of a $1/f^2$ law with a term proportional to f^4. This is true for all other experimental runs we have investigated. The results of the fitting are reported in Fig. 2. Coefficients and uncertainties are reported in Table I.

The same table reports the results for a run performed with the 40 mm PM, 2 mm gaps prototype. Both runs were performed with the same W torsion fiber.

TABLE I. Results of the estimate of excess noise.

Prototype	f^{-2} coefficient	f^4 coefficient
46 mm PM, 4 mm gaps	$(3.7 \pm 0.3) \times 10^{-36}$ N^2 m^2 Hz	$(3.8 \pm 0.4) \times 10^{-21}$ N^2 m^2/Hz^5
40 mm PM, 2 mm gaps	$(5.0 \pm 0.4) \times 10^{-36}$ N^2 m^2 Hz	$(1.3 \pm 0.2) \times 10^{-21}$ N^2 m^2/Hz^5

IV. DISCUSSION AND CONCLUSIONS

Figure 2 shows that excess noise only becomes negligible around 2–3 mHz. Below this frequency the $1/f^2$ term is a significant contribution to the noise that brings total noise to a value which is 40% above the background at 1 mHz and 2 times this one at 0.2 mHz. We have not yet understood the origin of this excess. There is no significant correlation with the magnetometer readout. A weak, barely significant correlation between $\bar{N}(t)$ and the thermometer monitoring the vacuum column enclosing the torsion fiber was found. This temperature was also correlated with the vertical motion $z(t)$ of the PM that consequently showed a correlation with $\bar{N}(t)$. A subtraction of this effect would lower the excess by only 10%.

A few considerations seem to indicate that the excess is a property of the pendulum and is not connected to the interaction between the PM and GRS. First the noise level has not been significantly affected by the change in the design of the GRS (Table I), with the difference between the results obtained with the two prototypes being well within the variability, of a factor ≈ 2, observed for each prototype among different runs taken at different times during the many-month campaigns performed in each case. This is true even though changing 2 mm to 4 mm gaps represents, as discussed, a major change, significantly reducing, for instance, the coupling between charge patches [7] and significantly increasing the gas molecular conductance around the PM.

A candidate source for the measured torque excess is connected with the continuous unwinding of the fiber due to creep in the fiber material. In the runs presented, the fiber unwound with a rate of $\approx 2 \times 10^{-10}$ rad/s. The rate is reduced by temperature annealing the fiber under load. Unfortunately we are limited by practical reasons to an annealing temperature of only $\approx 60°$ C. It is interesting to note that a simple Poisson model where single angular slip events of amplitude $\delta\phi$ contribute to both unwinding and the residual noise, yields a step size of $\delta\phi \approx 40$ nrad and a rate of $\approx 5 \times 10^{-3}$ s^{-1}.

We searched for evidence of such glitches by running a Wiener filter on the data matched to step-shaped torque signals. The filter resolution for angular steps, resulted to be $\sigma = 33$ nrad, roughly the size expected from the reasoning above. The filter did indeed detect several well-identified large amplitude (3–5σ) events, satisfying goodness-of-the fit test criteria, and which accounted for $\approx 20\%$ of the excess noise at low frequency.

One can even entirely suppress the excess noise at low frequency by subtracting the ≈ 200 highest events, with amplitude as low as $\pm 2\sigma$.

These results can be taken as an indication of angular glitches but not as an unambiguous proof and thus, for the sake of estimating an upper limit, such events have not been subtracted from the data of Fig. 2. It is worth remembering that any data series can be approximated with arbitrary precision by a sequence of variable amplitude steps and thus an incautious subtraction procedure can possibly, and erroneously, cancel the noise entirely.

The high frequency excess proportional to f^4 is also statistically significant. The excess is due to a residual correlation between the readouts at high frequency and had not been previously detected, as the cross-correlation technique was not available. We plot in Fig. 3 the real part of cross coherence $r(f) = \mathrm{Re}\{S_{\phi_{\mathrm{ac}},\phi_{\mathrm{GRS}}}(f)\}/\sqrt{S_{\phi_N}(f)S_{\phi_r}(f)}$ as the function of frequency. Data show that $r(f)$ is still 0.10 ± 0.02 at 10 mHz, dropping to non-significant values only above 60 mHz.

It would be truly difficult to attribute this excess to any real torque on the PM. For instance, when converted to a voltage on one of the electrodes, this would amount to a noise of 4 V/$\sqrt{\mathrm{Hz}}$ at 300 mHz assuming an unrealistically large dc voltage of 2 V on the same electrode, all figures unlikely by orders of magnitude [8].

The f^4 dependence converts into a white rotational noise of the entire apparatus relative to the local frame of inertia by ≈ 30 nrad/$\sqrt{\mathrm{Hz}}$. Thus a possible explanation may be

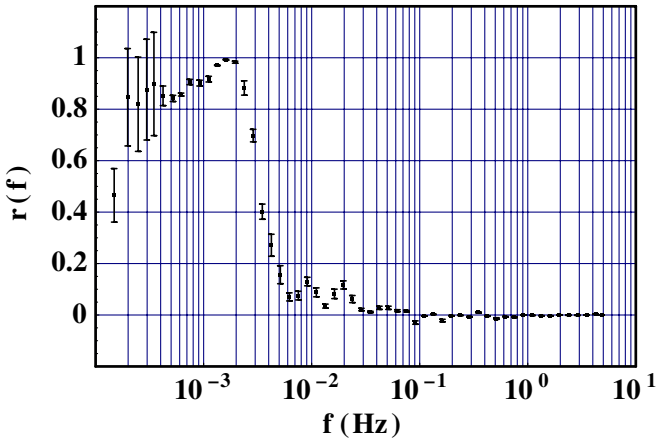

FIG. 3 (color online). Real part of cross coherence between autocollimator and GRS data.

such a rotation due either to seismic noise or to local mechanical distortion.

The observed variability of the effect (see for instance Table I) would make seismic noise at the laboratory site an unlikely explanation, while local mechanical distortion due to environmental variations and human activity remains possible. In addition a residual electrical cross talk between GRS and autocollimator cannot be excluded.

Though the detected excess is likely not due to the GRS itself and is not then relevant to LISA, we still include it when estimating the upper limit to the disturbances acting on the PM. This upper limit also includes the fit uncertainty and the uncertainty in the evaluation of thermal noise, conservatively estimated to be 20% and coming from the error in Q-factor measurement.

We express this torque upper limit as an equivalent acceleration noise based on a few simple assumptions on the contributing effects [5]. For instance simulations [5] give that randomly distributed normal forces, like those associated with parasitic electric fields, would exert both torque and force noise, with a ratio of their amplitudes of roughly 0.4 L, with L the PM size. This holds for disturbances with spatial exponential correlation lengths up to $L/10$. The ratio would decay to $L/4$ for a correlation slightly larger than L. $L/4$ is also the ratio obtained for an electrical disturbance applied to the electrodes of the x-face, as for electronic readout backaction. Finally forces acting tangentially, like diffuse scattering of molecules, show a ratio of $L/2$.

We then convert the upper limit from the data of Fig. 2 into an equivalent acceleration noise that the corresponding forces would exert on the 1.96 kg LISA PM by using the lowest ratio $L/4$, i.e. 10.7 cm (Fig. 4). The reader should be aware though that our pendulum geometry would not detect disturbances applied uniformly and normal across the x-face or tangentially to the y and z-faces, or disturbances acting normally onto the center of the x-face or in a few other symmetric positions.

Within the same figure we also report for comparison the acceleration level that would guarantee to LISA a measurement of the gravitational wave signal from a few binary systems in our Galaxy over 1 yr integration time. The signal amplitude is taken from Ref. [9] and the LISA sensitivity is averaged for source inclination and polarization.

It is important to stress again the limits of this observation.

Besides the lack of sensitivity to volume forces, all effects due to coupling among different DOF that would take place for a fully free-falling PM are absent here.

Additionally the environment on board LISA will be substantially different from the laboratory one, with a higher PM charging rate due to cosmic rays but with a lower level of temperature and magnetic field fluctuations. The effects of these disturbances, however, are well understood, have been investigated separately by dedicated experiments [8], and are found in good agreement with the expectations.

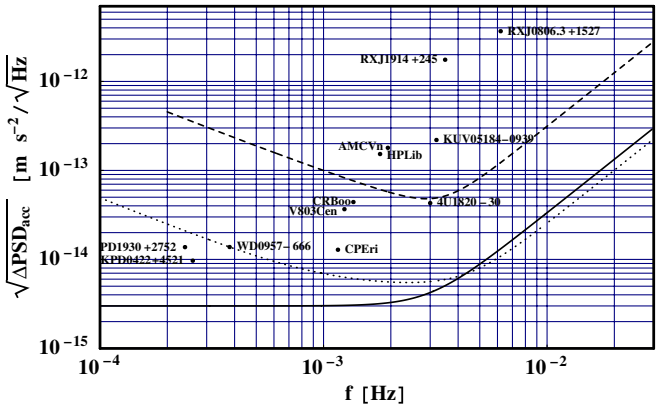

FIG. 4 (color online). Dashed line: upper limit to pendulum torque noise with GRS converted into equivalent acceleration on one of LISA proof masses. Dots: acceleration level required to detect with LISA, with signal-to-noise ratio of 1, the signal from the corresponding galactic binary system over 1 yr integration. Dotted line: projected upper limit for nonmodeled overall force disturbances from the LPF mission. Solid line: LISA requirements.

In Fig. 4 we also report the projected result of a comparable reduction process on the data from the LPF mission [3]. The mission will measure, by means of a laser interferometer, the relative acceleration of two LISA-like PMs in free fall within the same spacecraft.

Mission requirements call for a demonstration of relative acceleration of better than 3×10^{-14} (m/s$^2\sqrt{\text{Hz}}$) $\times \sqrt{1 + (f/3\ \text{mHz})^4}$ above 1 mHz. The relaxation of requirements relative to LISA is dictated by the need of keeping the test reasonably simple, but does not affect the GRS design. The current estimate [10] places the sensitivity better than requirements at $\approx 2 \times 10^{-14}$ (m/s$^2\sqrt{\text{Hz}}$), with the largest contributions being the cross talk with side motion of the PMs, actuation force fluctuations, magnetic fluctuations, and residual coupling to the spacecraft via force gradients. This last coupling, a subject of test in itself, can however be balanced between PMs in order to suppress the influence of the spacecraft jitter on their *relative* motion. PM side motion is measured with sufficient precision to allow for a subtraction similar to what we did with tilt in the case of the pendulum. LPF also carries magnetometers so that magnetic noise correction should be possible. With these largest entries suppressed this way, LPF may be able to put an upper limit on nonmodeled disturbances for a single PM acceleration of $\approx 5 \times 10^{-15}$ (m/s$^2\sqrt{\text{Hz}}$) at 1 mHz. Above ≈ 5 mHz interferometer noise will limit the sensitivity, while below 1 mHz noise degradation is expected to be no worse than a $1/f^2$. This is the rationale behind the curve shown in Fig. 4.

In conclusion, even at the present level of experimental knowledge, LISA should be able to detect bright gravitational wave signals. If LPF will meet its expected performance, the risk of a major unpredicted force will be almost entirely retired and LISA would have most of its planned science guaranteed.

[1] S. Vitale *et al.*, Nucl. Phys. B, Proc. Suppl. **110**, 209 (2002).
[2] R. T. Stebbins *et al.*, Classical Quantum Gravity **21**, S653 (2004).
[3] S. Anza *et al.*, Classical Quantum Gravity **22**, S125 (2005).
[4] R. Dolesi and S. Vitale, AIP Conf. Proc. **523**, 231 (2000).
[5] L. Carbone *et al.*, Phys. Rev. Lett. **91**, 151101 (2003).
[6] R. Dolesi *et al.*, Classical Quantum Gravity **20**, S99 (2003).
[7] C. C. Speake and C. Trenkel, Phys. Rev. Lett. **90**, 160403 (2003).
[8] L. Carbone *et al.*, Classical Quantum Gravity **22**, S509 (2005).
[9] E. Sterl Phinney *et al.*, "*LISA Science Requirements*," 2002 (unpublished), http://www.tapir.caltech.edu/listwg1/.
[10] "*Science Requirements and Top-level Architecture Definition for the LISA Technology Package LTPA-UTN-ScRD-Iss003-Rev1*," 2005 (unpublished).